衛星観測と地上観測

- AE
- DE
- DMSP
- Viking
- Freja
- Akebono
- Interball-Aurora
- Polar
- FAST
- IMAGE
- Cluster-II
- Reimei

- 全天オーロラカメラ
- （掃天・固定）フォトメータ
- 狭視野カメラ

地上オーロラ発光観測装置-1

スウェーデン・ALIS

昭和基地・全天カメラ

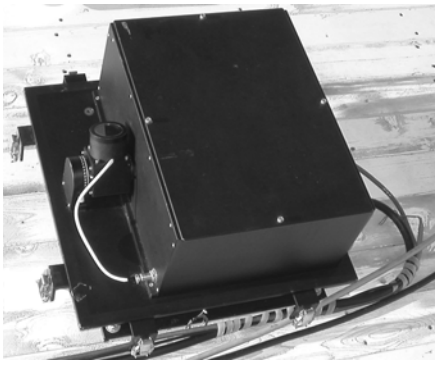

昭和基地・固定フォトメーター

昭和基地・掃天フォトメーター

昭和基地・狭視野カメラ

提供：極地研・麻生名誉教授、門倉教授

地上オーロラカメラの観測例

狭視野テレビカメラによるオーロラ微細構造の観測

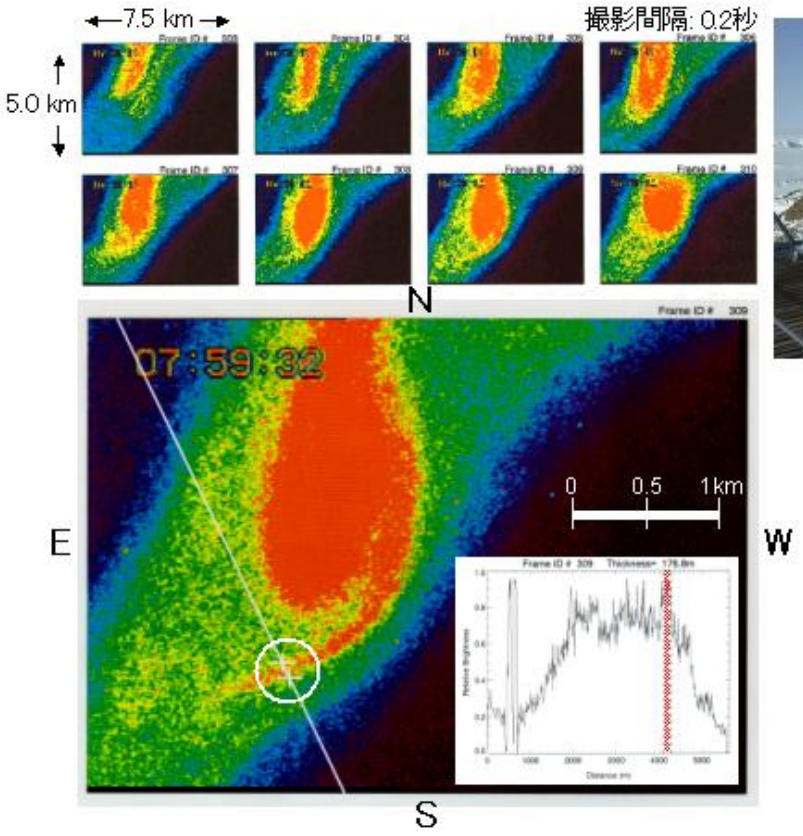

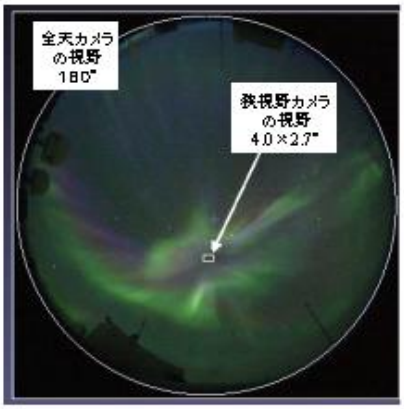

提供：極地研・宮岡准教授

地上オーロラ発光観測装置-2

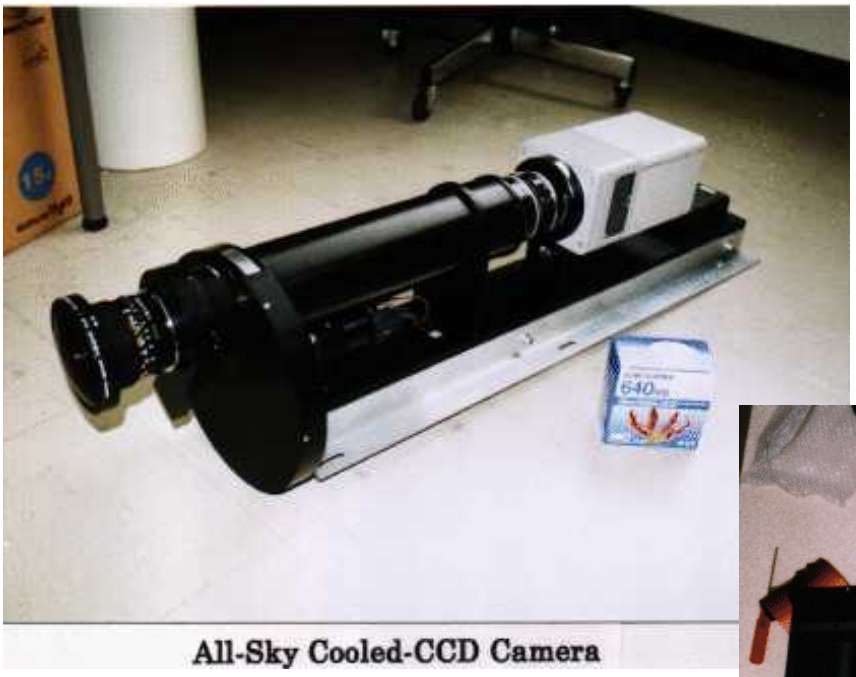

All-Sky Cooled-CCD Camera

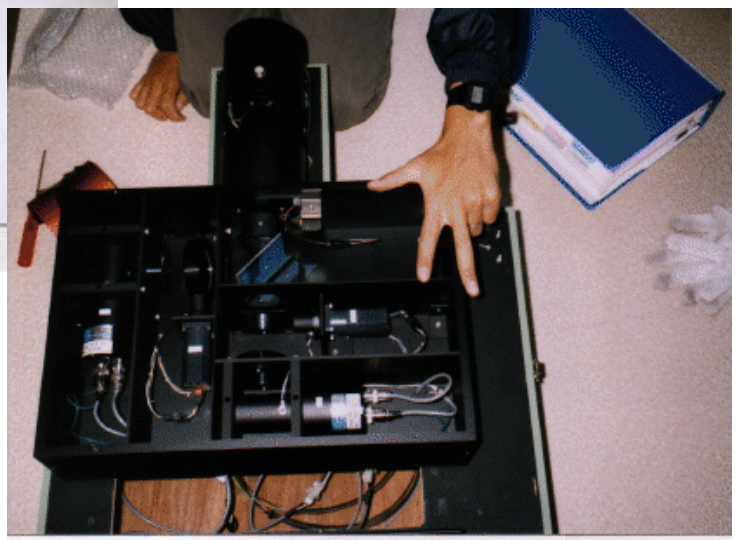

Two-Channel Tilting Photometer

提供：名古屋大学・塩川教授

全天オーロラカメラ

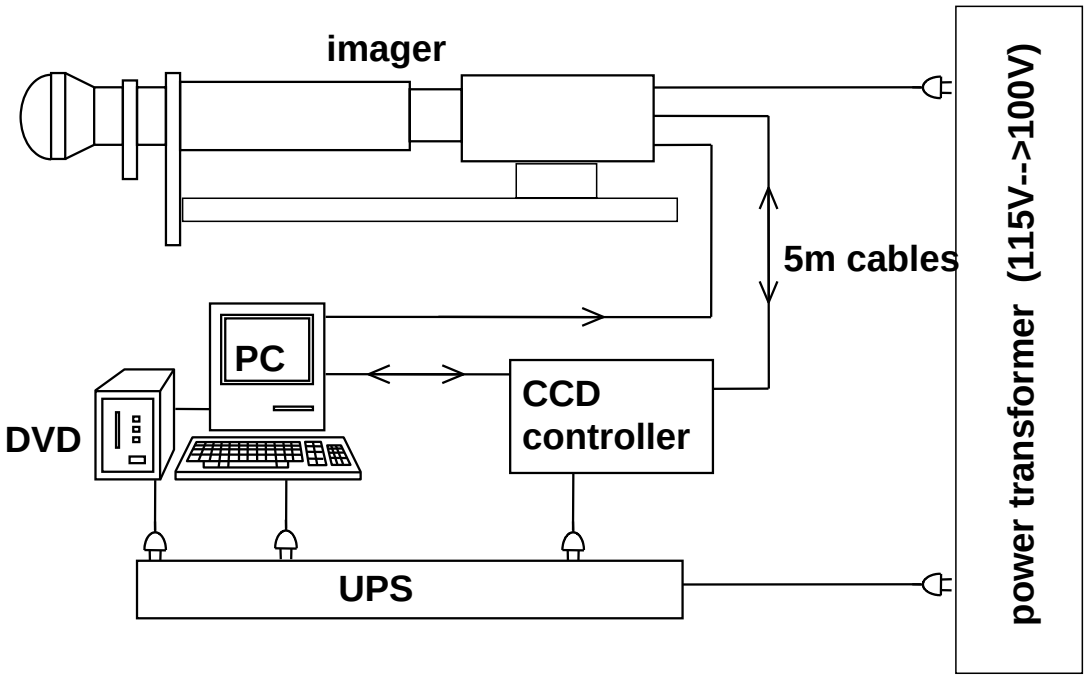

提供：名古屋大学・塩川教授

地上オーロラ発光観測装置-3

カナダ・アサバスカ

提供：名古屋大学・塩川教授

地上オーロラ発光観測装置-4

南極点基地：全天イメージャー

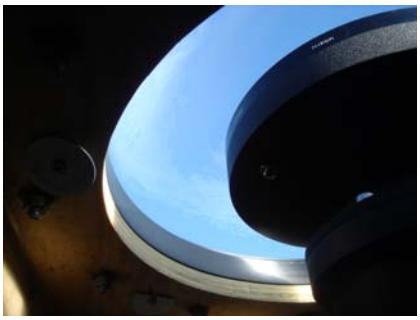

提供：京都大学・海老原助教授

Sept.5, 2005
Athabasca

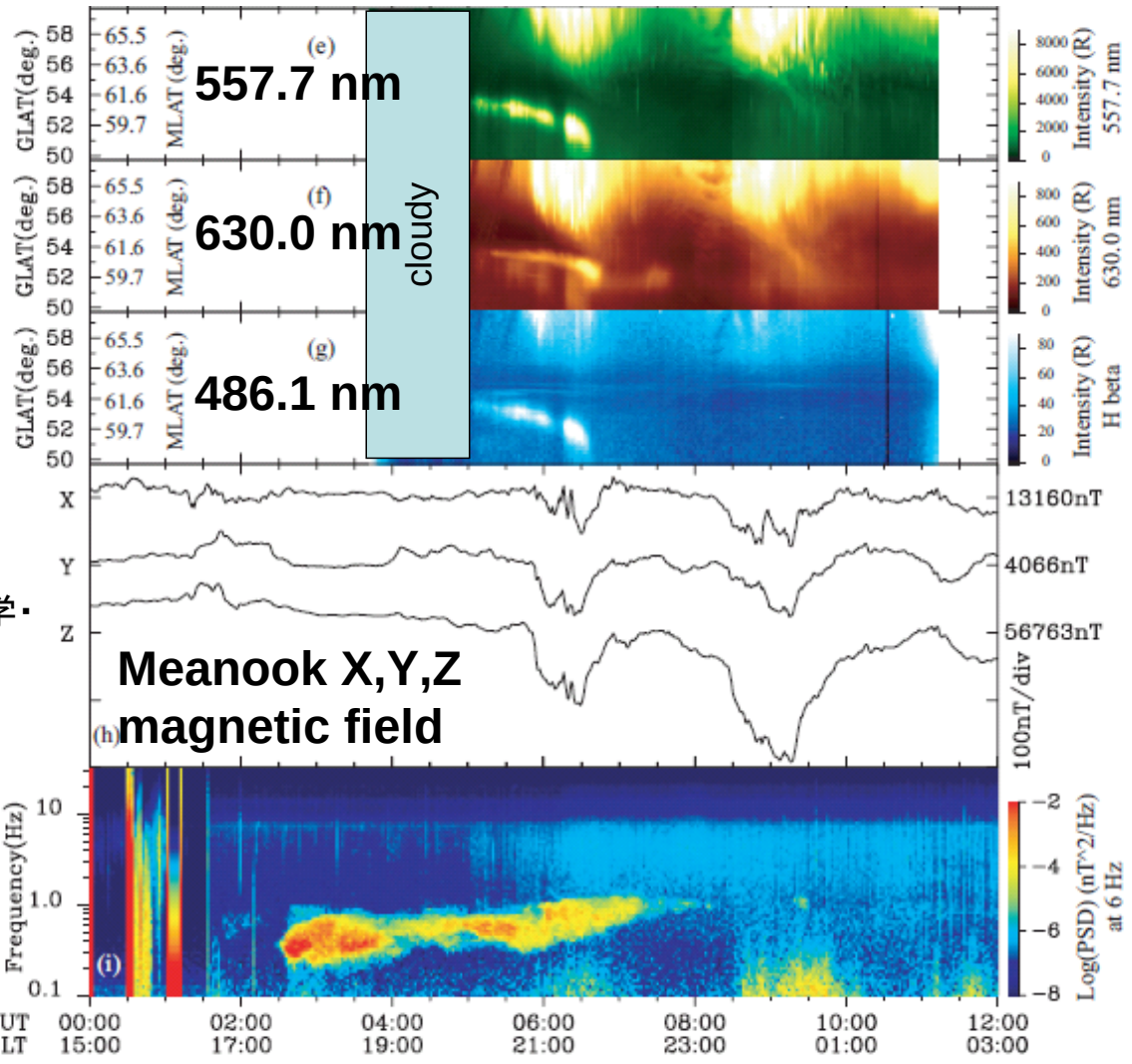

提供：名古屋大学・
塩川教授

dH/dt
0.1-32Hz

Sakaguchi et al.
(JGR, 2007)

人工衛星によるオーロラ観測

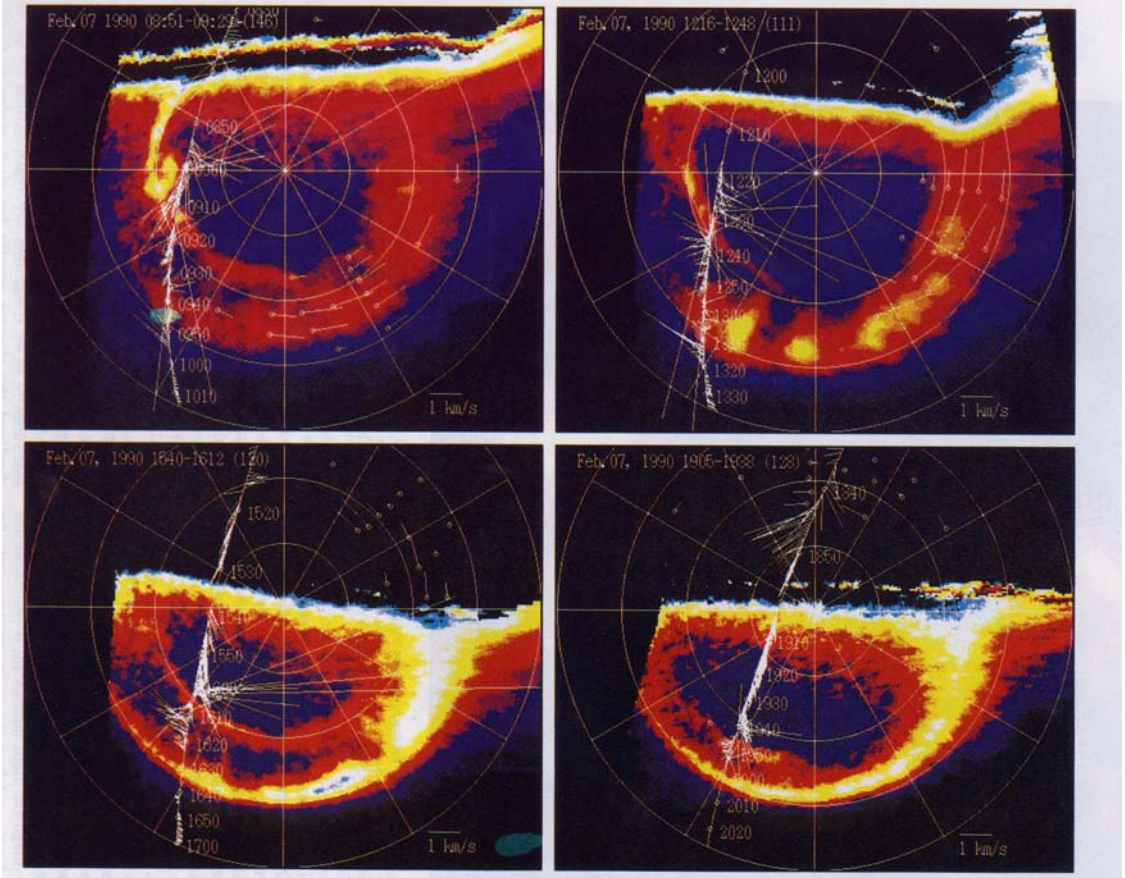

Plate 1. Polar plots of UV-auroral images for the successive four orbits on February 7, 1990, along with the trajectory of the satellite magnetic foot point, convection velocity vectors estimated from the in situ measurement of electric field, and equivalent convection vectors from the magnetic field deflection on the ground, reproduced by rotating the horizontal deflection vectors counterclockwise by 90°. The corrected geomagnetic coordinate and the magnetic local time are used throughout this paper. The magnetic pole is at the center of the image, midnight at the bottom center, and dusk at the middle left. The latitude circles are drawn every 10°. Each image is reproduced by averaging all the images obtained during the corresponding orbit. The time interval and the number of images averaged are indicated in each panel.

極域磁気圏での粒子と沿磁力線電流の観測-1

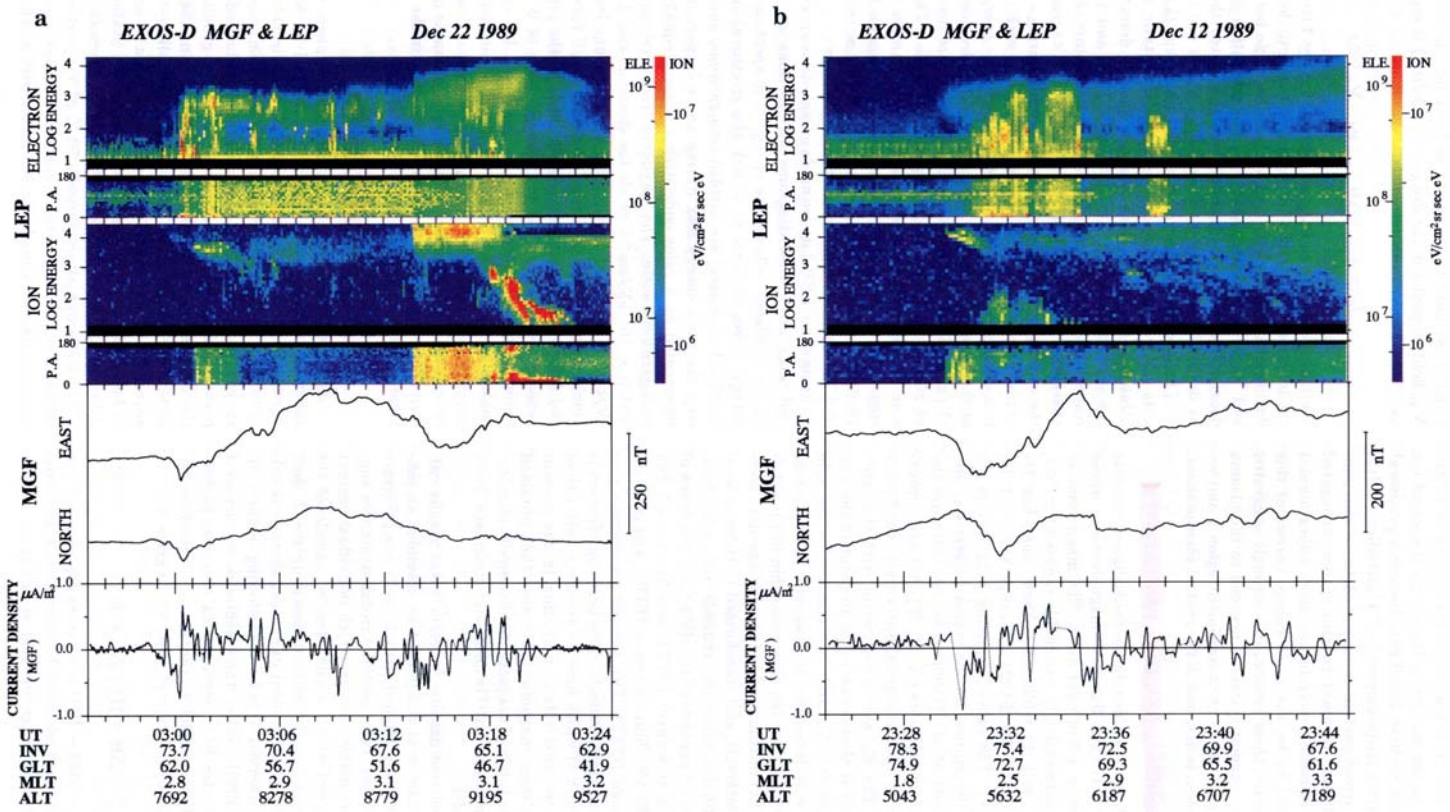

Plate 1. Energy–time spectrograms and pitch angle–time diagrams for electrons and ions and magnetic field perturbations and current densities obtained from the EXOS D postmidnight observations on (*a*) December 22, 1989, (*b*) December 12, 1989, (*c*) December 18, 1989, and (*d*) January 9, 1990.

極域磁気圏での粒子と沿磁力線電流の観測-2

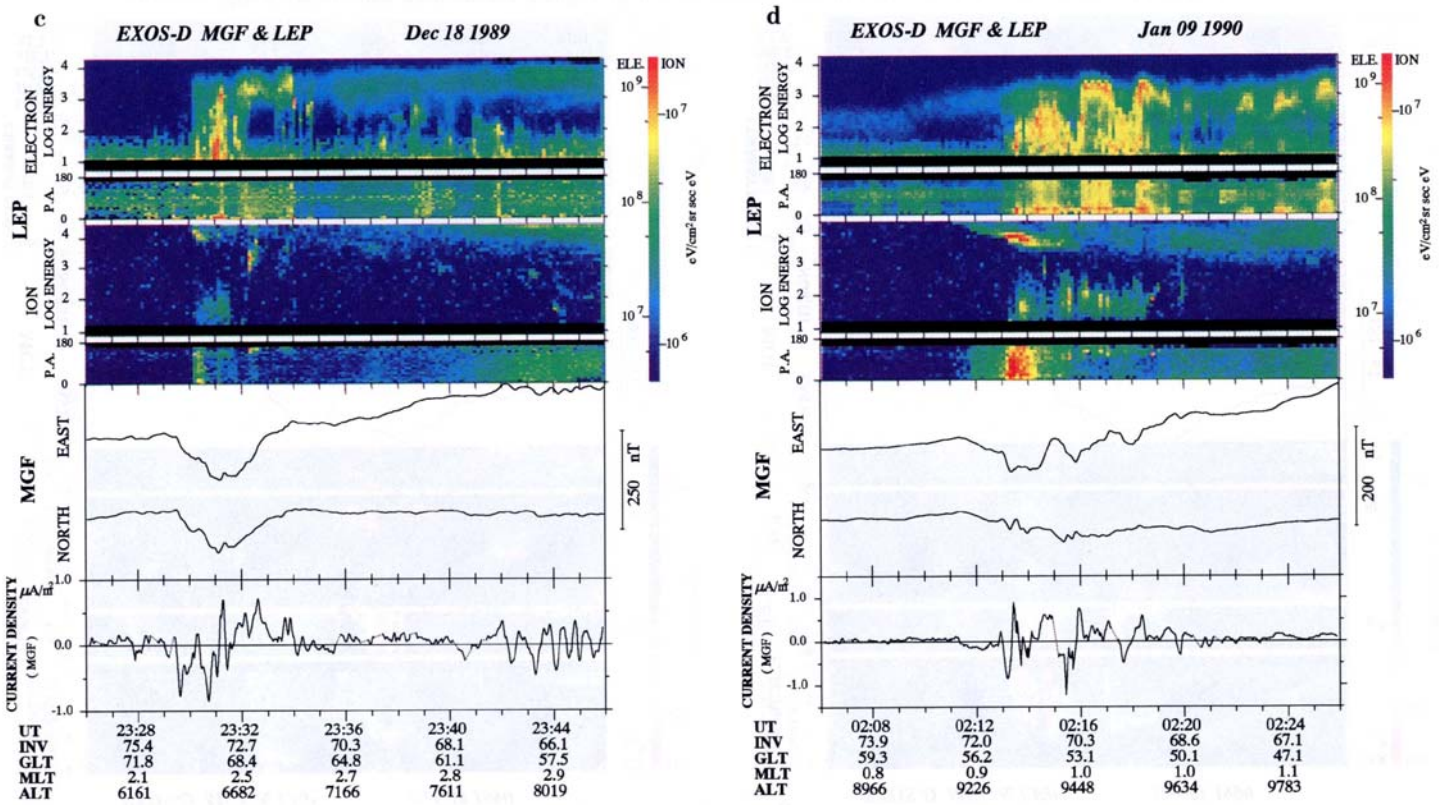

Plate 1. (Continued)

極域磁気圏での粒子観測-1

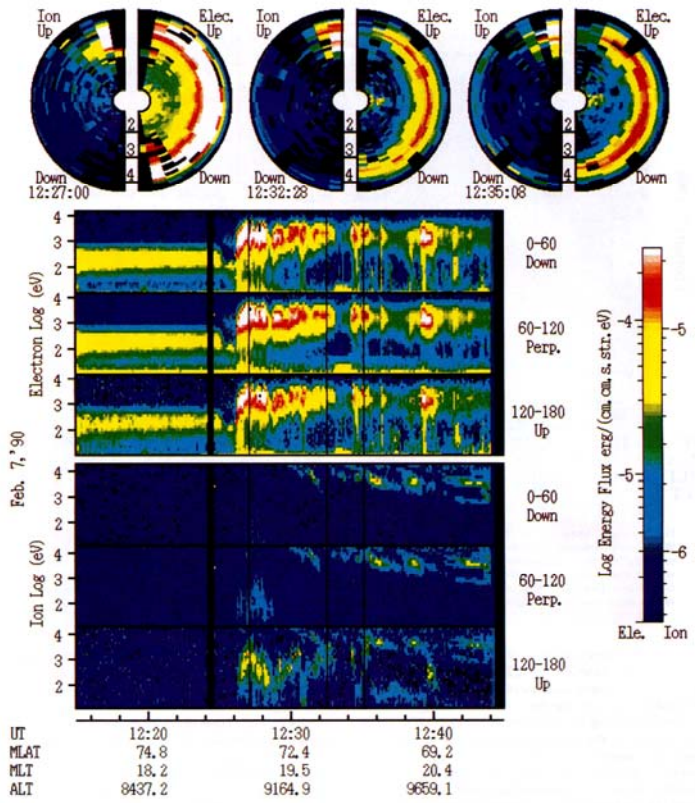

Plate 3. Polar displays of electron/ion distribution functions at the three selected times (top panels), and pitch-angle sorted electron and ion energy-time spectrograms (bottom panels). In the energy-time spectrograms, from the top are displayed the electron spectra for pitch angles of 0°-60° (downward), 60°-120° (perpendicular), and 120°-180° (upward), followed by the ion spectra for the same ranges of pitch angles as those for electrons, for 1215-1244 UT on February 7, 1990. In the polar displays, the right and left halves show the electron and ion distributions, respectively. The black portion indicates the lack of observation or negligibly small count rates. Electron spectra show the accelerated precipitations from 1226 to 1234 UT. After 1234 UT they turn to more continuous unstructured ones although some enhancements in flux take place several times. Between 1226 and 1229 UT, electrons with energy lower than several hundreds of keV are observed, while they disappear after 1229 UT (spectral hole). The ion spectra also show the change from conical distributions to UFI beam at 1229 UT.

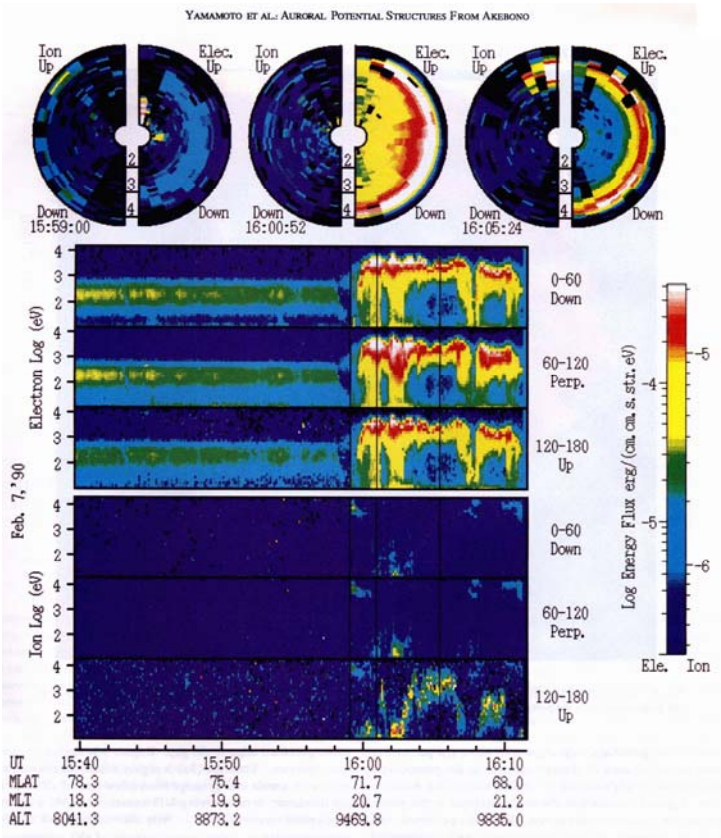

Plate 5. Same as Plate 3 but for 1540-1611 UT on February 7, 1990. The change in ion spectra from the conical distributions to UFI beams is still seen at the poleward edge of the discrete aurora (1603 UT). The electron hole distribution (the lack of lower-energy population) is evident inside the discrete aurora. Dispersive ions and low-energy counterstreaming electrons are observed at the poleward edge of the accelerated electron region (1559 UT).

極域磁気圏での粒子観測-2

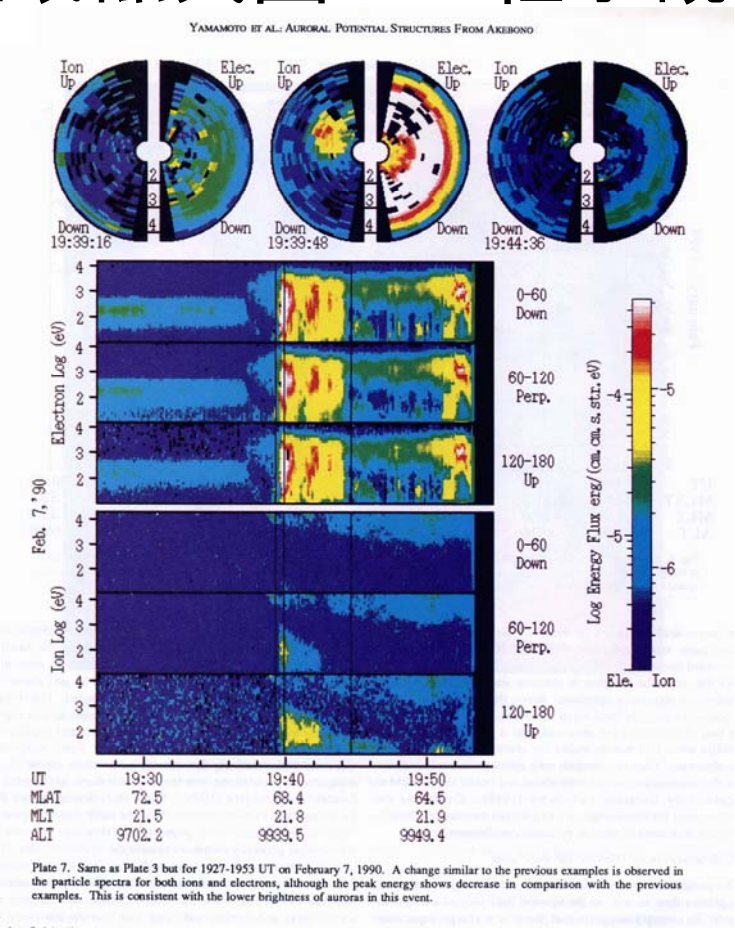

Plate 7. Same as Plate 3 but for 1927-1953 UT on February 7, 1990. A change similar to the previous examples is observed in the particle spectra for both ions and electrons, although the peak energy shows decrease in comparison with the previous examples. This is consistent with the lower brightness of auroras in this event.

極域磁気圏での粒子と沿磁力線電流の特徴

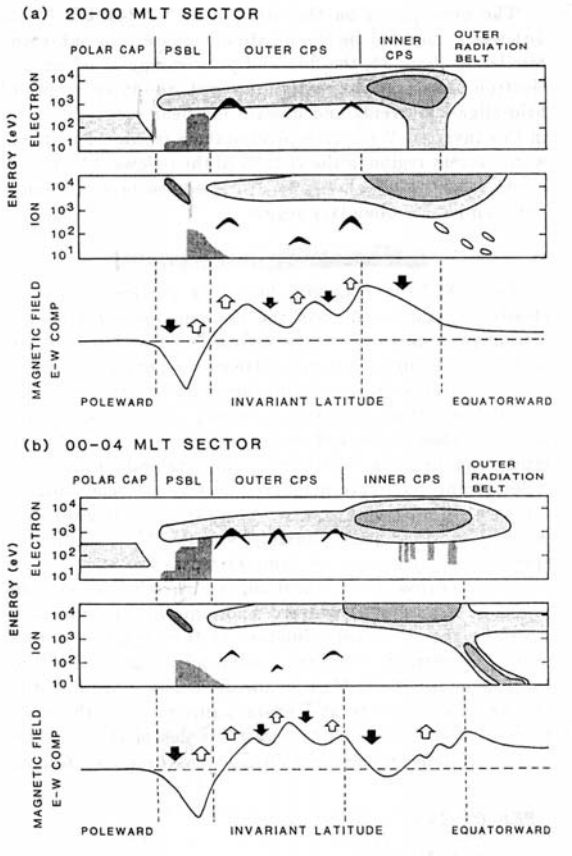

Fig. 7. Schematic diagrams showing the spatial relationships between field-aligned currents and charged particles observed on EXOS D during moderate magnetic activity for (*a*) the 20–00 MLT sector and (*b*) the 00–20 MLT sector. Downward and upward arrows denote field-aligned currents flowing into and out of the ionosphere, respectively.

領域分類

- BPS (Boundary Plasma Sheet)
- CPS (Central Plasma Sheet)
- PSBL (Plasma Sheet Boundary Layer)

特徴的な粒子分布

- Polar Shower
- Polar Rain
- Polar Wind
- VDIS
- Bouncing Ion Cluster (Dipolarization, UFI)

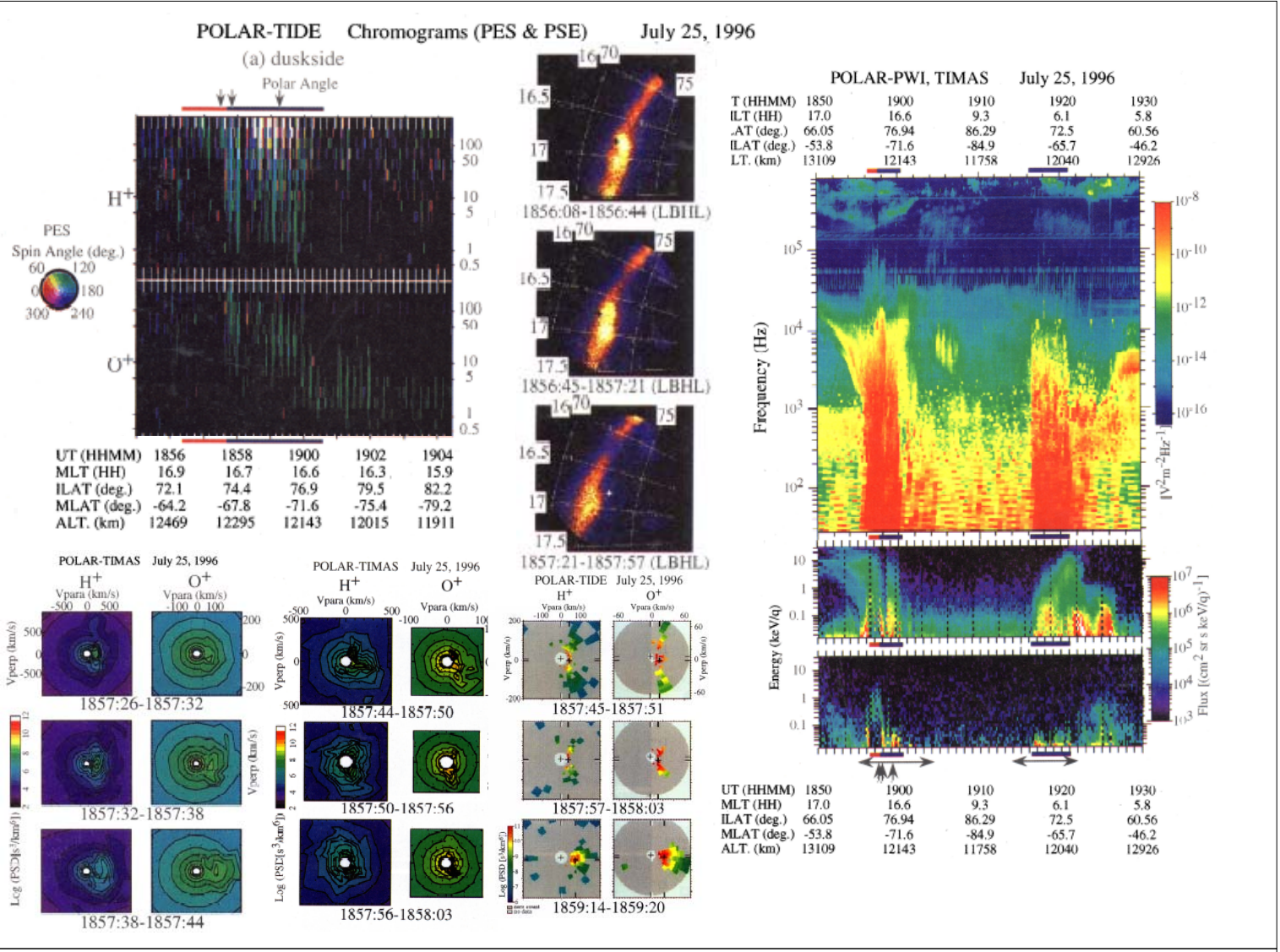
POLAR-TIDE Chromograms (PES & PSE) July 25, 1996
(a) duskside
Polar Angle
H+
O+
PES
Spin Angle (deg.)
UT (HHMM) 1856 1858 1900 1902 1904
MLT (HH) 16.9 16.7 16.6 16.3 15.9
ILAT (deg.) 72.1 74.4 76.9 79.5 82.2
MLAT (deg.) -64.2 -67.8 -71.6 -75.4 -79.2
ALT. (km) 12469 12295 12143 12015 11911
1856:08-1856:44 (LBHL)
1856:45-1857:21 (LBHL)
1857:21-1857:57 (LBHL)
POLAR-PWI, TIMAS July 25, 1996
T (HHMM) 1850 1900 1910 1920 1930
ILT (HH) 17.0 16.6 9.3 6.1 5.8
AT (deg.) 66.05 76.94 86.29 72.5 60.56
ILAT (deg.) -53.8 -71.6 -84.9 -65.7 -46.2
LT. (km) 13109 12143 11758 12040 12926
Frequency (Hz)
Energy (keV/q)
UT (HHMM) 1850 1900 1910 1920 1930
MLT (HH) 17.0 16.6 9.3 6.1 5.8
ILAT (deg.) 66.05 76.94 86.29 72.5 60.56
MLAT (deg.) -53.8 -71.6 -84.9 -65.7 -46.2
ALT. (km) 13109 12143 11758 12040 12926
POLAR-TIMAS July 25, 1996
H+
O+
Vpara (km/s)
Vperp (km/s)
1857:26-1857:32
1857:32-1857:38
1857:38-1857:44
1857:44-1857:50
1857:50-1857:56
1857:56-1858:03
POLAR-TIDE July 25, 1996
1857:45-1857:51
1857:57-1858:03
1859:14-1859:20

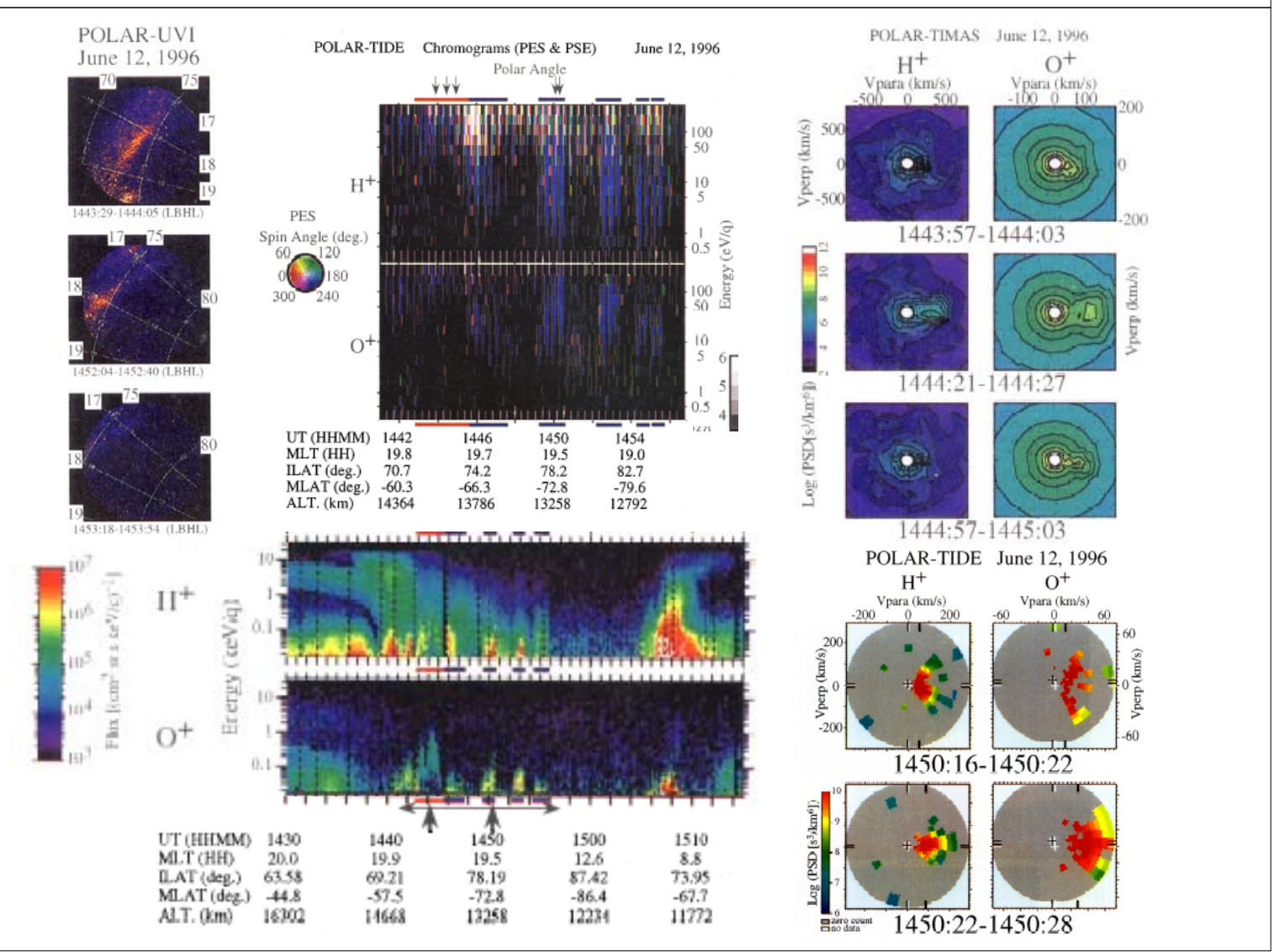
POLAR-UVI
June 12, 1996
1443:29-1444:05 (LBHL)
1452:04-1452:40 (LBHL)
1453:18-1453:54 (LBHL)
POLAR-TIDE Chromograms (PES & PSE) June 12, 1996
Polar Angle
H+
O+
PES
Spin Angle (deg.)
Energy (eV/q)
UT (HHMM) 1442 1446 1450 1454
MLT (HH) 19.8 19.7 19.5 19.0
ILAT (deg.) 70.7 74.2 78.2 82.7
MLAT (deg.) -60.3 -66.3 -72.8 -79.6
ALT. (km) 14364 13786 13258 12792
POLAR-TIMAS June 12, 1996
H+
O+
Vpara (km/s)
Vperp (km/s)
1443:57-1444:03
1444:21-1444:27
1444:57-1445:03
POLAR-TIDE June 12, 1996
1450:16-1450:22
1450:22-1450:28
UT (HHMM) 1430 1440 1450 1500 1510
MLT (HH) 20.0 19.9 19.5 12.6 8.8
ILAT (deg.) 63.58 69.21 78.19 87.42 73.95
MLAT (deg.) -44.8 -57.5 -72.8 -86.4 -67.7
ALT. (km) 16302 14668 13258 12234 11772

Outflows of heavy cold ions in the plasma sheet at dipolariation

Event on November 8, 1998

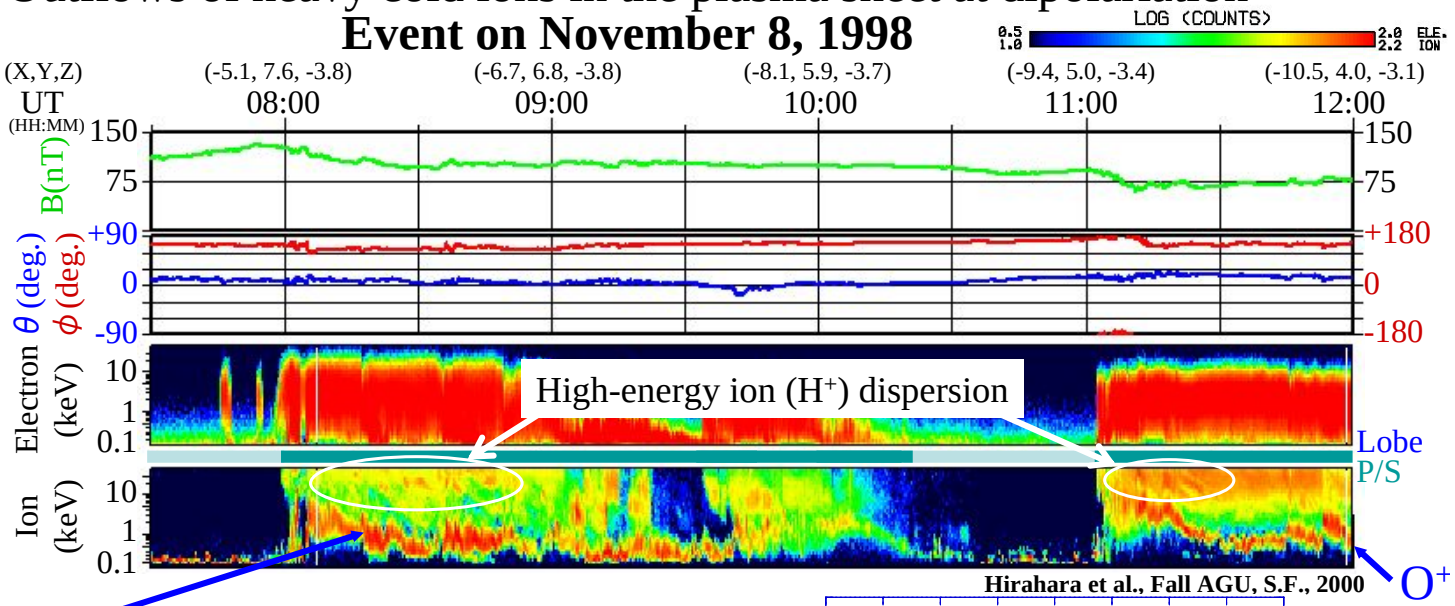

During the long storm time
Dipolarization & O^+ outflow
Weak He^+ & H^+ outflows

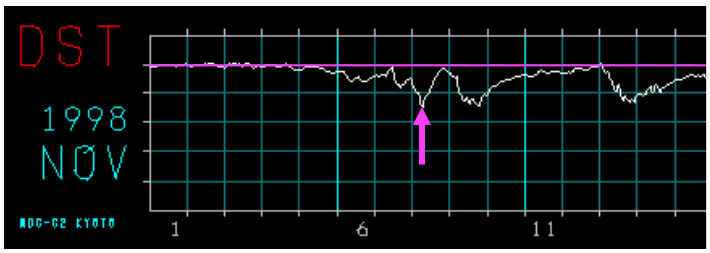

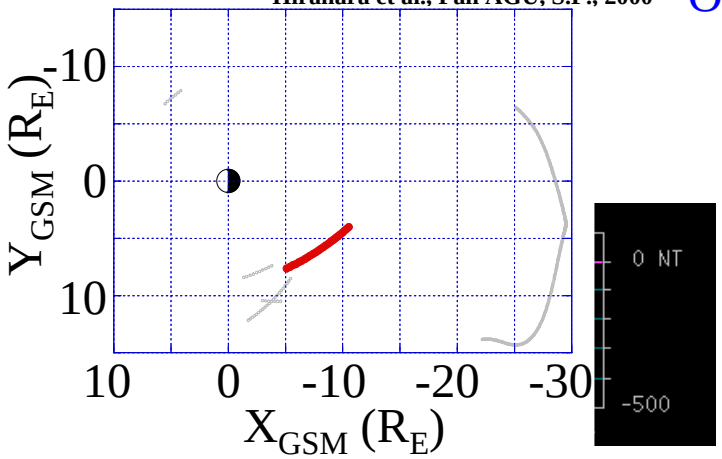

Beam-like signatures of O^+/He^+ outflow and counter-streaming O^+ beam at dipolarization event in the plasma sheet

Event on November 8, 1998

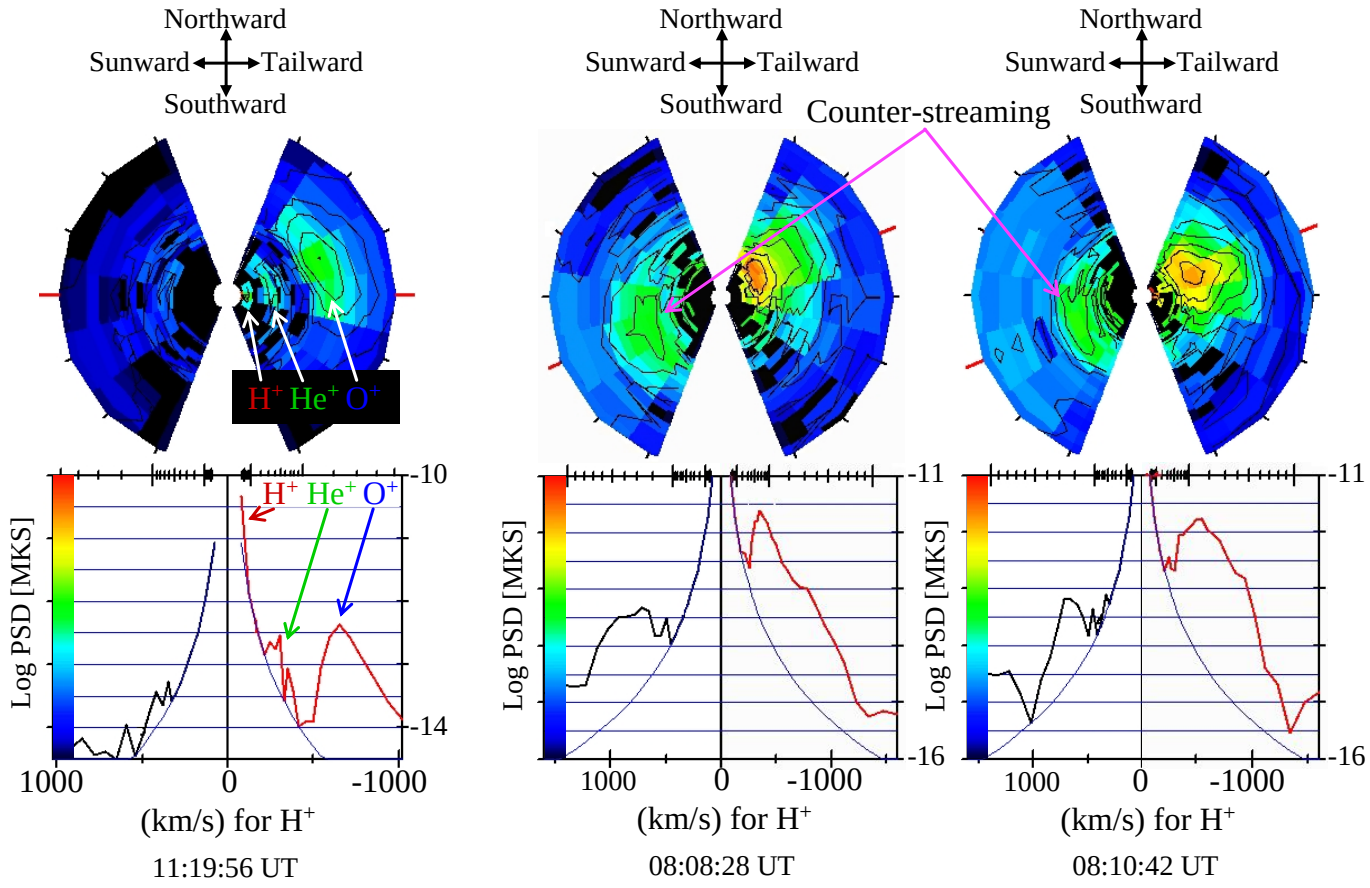

Outflows of heavy cold ions in the plasma sheet at dipolariation

Event on October 22, 1999

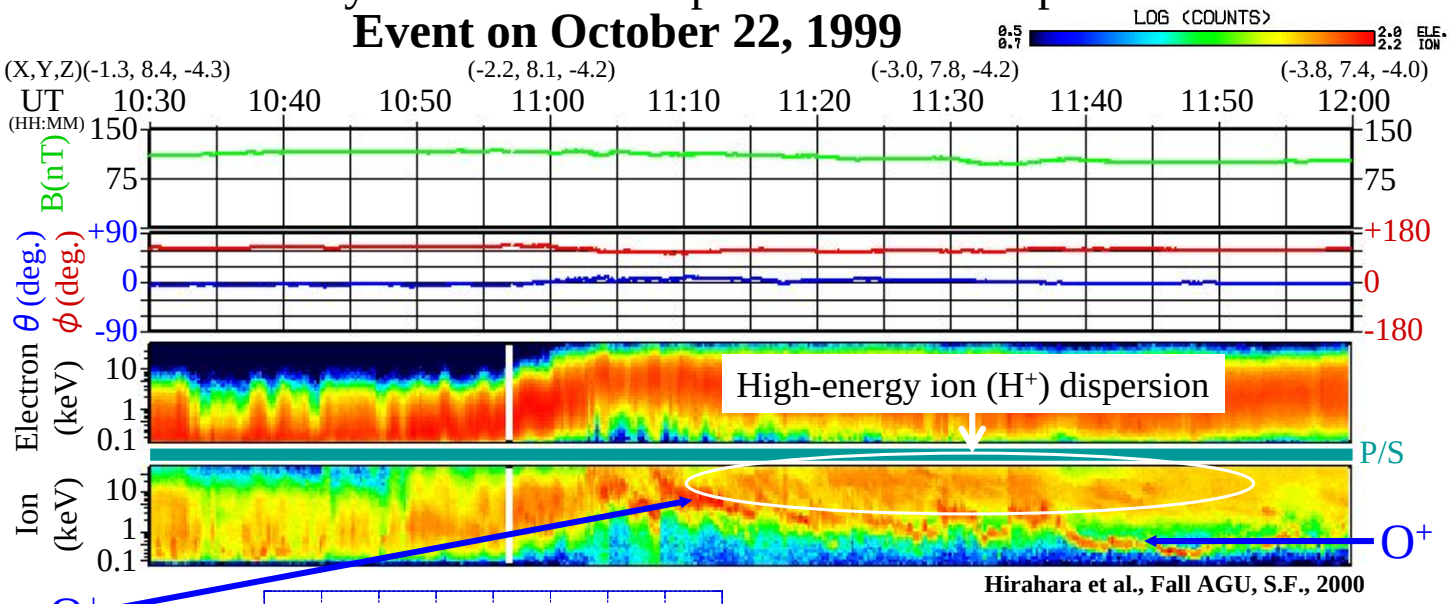

Hirahara et al., Fall AGU, S.F., 2000

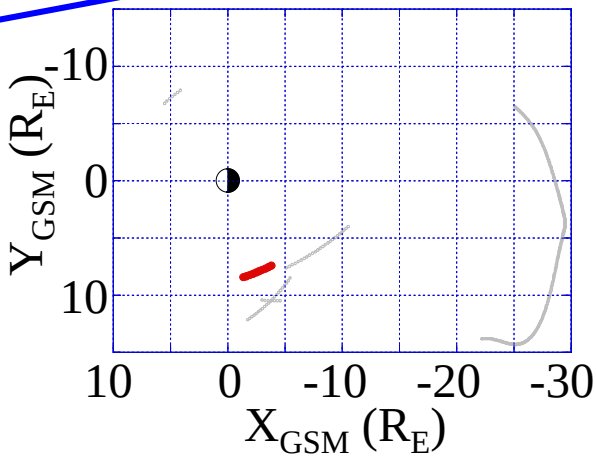

At the strong storm time
Dipolarization & O^+ outflow
Weak He^+ & H^+ outflows

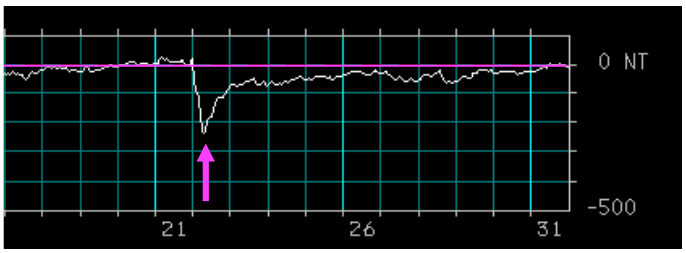

Beam-like signatures of O^+/He^+ outflow, and O^+ density, speed, and flux at dipolarization event in the plasma sheet

Event on October 22, 1999

11:05-11:14 & 11:39-12:00 UT
Density: 0.05-0.3/cm^3
(Average: 0.17/cm^3)
Speed : 50-300 km/s
(Average: ~100 km/s)

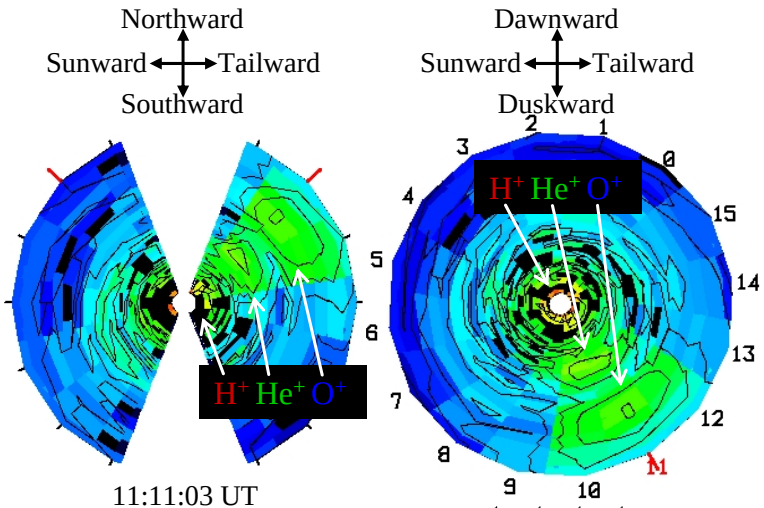

11:11:03 UT

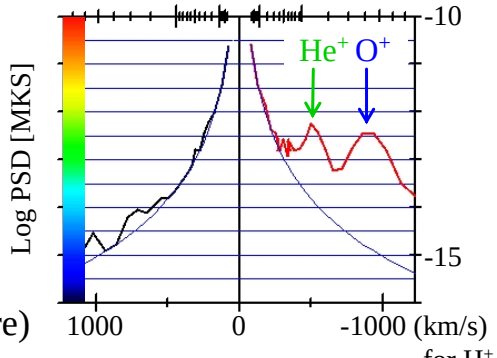

<u>Rough estimate of total outflowing O^+ ions</u>

Area with outflows : $2\pi \times 8\ R_E \times 1\ R_E \times (90^\circ/360^\circ)$
(a quadrant of ring shape at the equator)

Outflowing O^+ flux : $0.17/cm^3 \times 100$ km/s

Total outflowing O^+ ions : 0.9×10^{25} ions/s (from one hemisphere)
1.7×10^{25} ions/s (from both of hemisphere)